Article:
Luo, J, Long, X, Bowyer, FT et al. (6 more authors) (2021) Pulsed oxygenation events drove progressive oxygenation of the early Mesoproterozoic ocean. Earth and Planetary Science Letters, 559. 116754. ISSN 0012-821X

https://doi.org/10.1016/j.epsl.2021.116754

Supplementary Information

Carbonate Mineralogy

Figure S1 shows selected photomicrographs of representative samples from the Gaoyuzhuang Formation. Gaoyuzhuang Member I samples are well-preserved dolostones with ~2% euhedral Fe-oxides (hematite) and ~1% detrital minerals (Fig. S1 A,B). Some samples from the lower part of Member I also preserve original algal laminae (Fig S1, C). Samples from Gaoyuzhuang Member II are medium-fine grained dolostones, with less than 1% being fine-grained (average diameter of 20-50 μm) euhedral Fe-oxides and detrital minerals (e.g., quartz; Fig. S1, D, E). Gaoyuzhuang Member III is dominated by micritic dolostone with crystals of euhedral and sub-euhedral dolomite (generally less than 10 μm; Fig. S1 G,H). Samples from Gaoyuzhuang Member IV are characterized by coarse-grained dolostone (~100 μm) with ~10% fine crystals of euhedral dolomite (~10-20 μm).

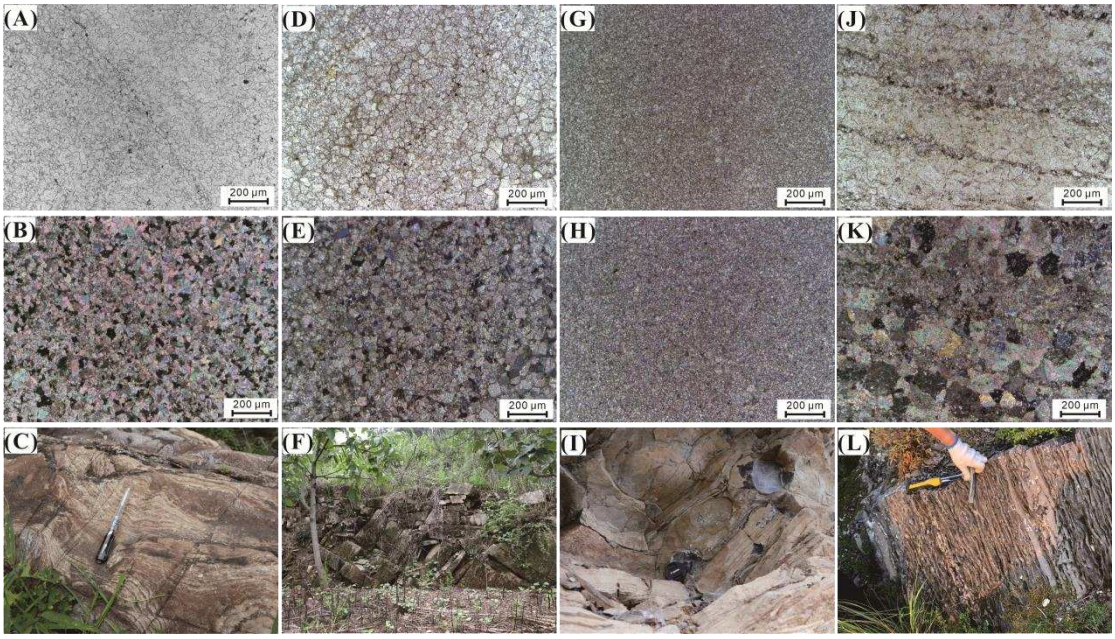

Figure S1. Selected photomicrographs of representative samples and outcrop pictures from the Gaoyuzhuang Formation. A, D, G and J were taken under plane polarized light, and B, E, H and K were taken under cross polarized light. (A, B, C), (D, E, F), (G, H, I), (J, K, L) are from Members I-IV, respectively. Detailed description of micrographs is discussed above. For outcrop pictures: (C) well preserved algal laminae from lower Member I; (F) Thick Mn-rich dolomite bed from Member

II, both of which are rich in manganese; (I) nodular structure preserved in lower Member III; (L) typical bituminous limestone from lower Member IV.

Materials and methods

In this study, 71 outcrop samples were collected from the Gaoyuzhuang Formation in the type section of Jixian County (40.0439° N, 117.4008° E). Due to poor exposure throughout much of the area, sampling was focused at the boundaries between individual members, which are clearly marked. Weathered surfaces were removed and fresh hand specimens with no visible evidence for alteration or veining were ultrasonically cleaned in distilled water, dried and milled to powder (<74 μm) using an agate mortar. Microscope images of representative samples are shown in the Figure S1.

1. Major and trace element concentrations

Major elements were determined via X-ray fluorescence (XRF) using a Rigaku ZSX100e spectrometer on glass disks, after ~0.5 g of whole-rock powder was fused with $Li_2B_4O_7$ + $LiBO_2$ + LiBr. Replicate analyses of international standards BHOV-2 and AGV-2 were consistent with certified values, yielding analytical uncertainties of ≤5% (~1% for SiO_2, ~5% for MnO_2 and Fe_2O_3, and ~2% for other major element oxides). For trace element analysis (Mn, Mo, Sr), ~50 mg of sample powder was dissolved in 0.5 ml concentrated HNO_3 and 1.0 ml of HF in high pressure Teflon-coated steel bombs, and heated at 195°C for 24 h. Solutions were measured using an Agilent Technologies 7700x quadrupole ICP–MS. Rock standards W-2, AGV-2, BHVO-2 and GSP-2 were used to calibrate elemental concentrations. Deviation from certified values was <10%.

2. Iron speciation

Iron speciation quantifies the fraction of total iron (Fe_T) that is highly reactive (Fe_{HR}) towards sulfide-promoted reductive dissolution (Raiswell and Canfield, 1998). The Fe_{HR} pool targets Fe

bound in carbonates (Fe_{carb}), ferric (oxyhydr)oxide minerals (Fe_{ox}), magnetite (Fe_{mag}) and iron sulfides (Fe_{py}; dominantly pyrite). Calibration of the iron speciation proxy in modern and ancient sediments demonstrates that Fe_{HR}/Fe_T <0.22 is commonly indicative of deposition under oxic water column conditions (Poulton and Canfield, 2011). By contrast, Fe_{HR}/Fe_T >0.38 commonly occurs due to water column precipitation and settling of Fe_{HR} minerals under anoxic water column conditions (Raiswell and Canfield, 1998). Where anoxic depositional conditions are inferred from Fe_{HR}/Fe_T >0.38, Fe_{py}/Fe_{HR} may be used to differentiate ferruginous (<0.6) from euxinic (>0.8) conditions (Poulton and Canfield, 2011; Benkovitz et al., 2020; Poulton, 2021). Carbonate rocks that have not been subjected to deep burial dolomitization and have total Fe concentrations >0.5 wt% are considered suitable for palaeoredox interpretation via Fe speciation (Clarkson et al., 2014). This minimum Fe_T threshold concentration accounts for the potential to record Fe_{HR} inputs that are unrelated to enrichments arising from mineral precipitation in an anoxic water column (Clarkson et al., 2014). Carbonates that fulfil the above criteria, and have not experienced additional Fe input during deep burial dolomitization, have been shown to faithfully record palaeoredox data consistent with contemporaneous shales (Clarkson et al., 2014). Previous petrographic observations of dolomite from the Gaoyuzhuang Formation show little evidence for deep burial dolomitization, with the exception of some dolomite samples from Member IV (Zhang et al., 2018). However, samples from Member IV have Fe_T <0.5 wt% and were not analysed for Fe speciation (Fig. 2).

Iron speciation analyses followed the sequential extraction procedure of Poulton and Canfield (2005). An initial leach using Na acetate buffered to pH 4.5 (48 h, 50°C) targeted Fe_{carb}, followed by Na dithionite (2 h, room temperature) to quantify Fe_{ox}, and an ammonium oxalate extraction (6 h, room temperature) to quantify Fe_{mag}. Sequential extraction solutions were measured via flame atomic

absorption spectrometry. The accuracy of extractions was confirmed relative to an international reference material (WHIT; Alcott et al., 2020), and replicate analyses (n = 6) yielded RSDs of 1.0% for Fe_{carb}, 2.7% for Fe_{ox}, and 1.3% for Fe_{mag}. The concentration of Fe_{py} was determined stoichiometrically on Ag_2S precipitates produced during a boiling chromous chloride distillation (Canfield et al., 1986), with a RSD of <5%.

3. Total organic carbon

Total organic carbon (TOC) concentrations were measured by combustion using a LECO CS-344 carbon-sulfur analyser. Samples were fully decarbonated prior to analysis using 1 M HCl, and residues were then washed with ultrapure 18.2 MΩ H_2O to ensure the removal of any remaining acid (pH >4). Samples were calibrated against a reference material (IFP160000), with a RSD of <5%.

4. Molybdenum isotopes

Samples with >50 ppb Mo were analyzed for δ^{98}Mo using ^{97}Mo-^{100}Mo double spike methods outlined in Li et al. (2014) and Zhao et al. (2016), at the State Key Laboratory of Isotope Geochemistry, Guangzhou Institute of Geochemistry, Chinese Academy of Science, and Mo concentrations were re-analysed separately during the isotope analysis process. Approximately 0.1–2.8 g of sample powder was accurately weighed and combined with the ^{97}Mo-^{100}Mo double spike in 15 ml PFA (perfluoroalkoxy ethylene) beakers (for sample weights <2 g) or 50 ml centrifuge tubes (for sample weights >2 g). Samples were then digested in 6 mol l^{-1} HCl at room temperature for >24 h. Mo separation and purification was achieved using N-benzoyl-N-phenyl hydroxylamine chromatographic resin (Li et al., 2014). Prior to use, the resin columns were washed with 10 ml Milli-Q water, 2 ml of 6 mol l^{-1} HF, Milli-Q water and 1 mol l^{-1} HCl. The sample solution was loaded onto the column with 0.45 μm filter membranes, and the resin was washed four times with 2 ml of 1 mol

l^{-1} HCl and four times with 2 ml of 0.2 mol l^{-1} HF. Finally, the adsorbed Mo was eluted four times with 2 ml of 6 mol l^{-1} HF. Acid solutions containing the purified Mo were collected in 15 ml PFA vials and dried on a hot plate at 120°C. One drop of purified concentrated HNO_3 and 2 drops of H_2O_2 were introduced to the PFA vials to oxidize the organic residue, and this process was repeated until the sample colour changed to white or pale yellow, reflecting complete dissolution of the organic residue. Following this, one drop of double-distilled concentrated HNO_3 and 0.5 ml of Milli-Q water were added to the vials.

After the separation and purification of Mo, isotopic ratios were determined on a Thermo-Fisher Scientific NeptunePlus multiple collector inductively coupled plasma mass spectrometer in the State Key Laboratory of Continental Dynamics, Northwest University. The isotopic composition of Mo was expressed as $\delta^{98/95}$Mo relative to the NIST SRM 3134 standard. The NIST SRM 3134 standard solution and two rock reference materials (marine sedimentary BGW 07-316 and carbonate COQ-1) were repeatedly measured along with the samples. The double spike calculation was performed using an in-house created Microsoft Virtual Basic program based on a mathematical algorithm presented in Zhang et al. (2015). Over the period of this study, standard/spike mixtures (^{98}Mo/^{100}Mo) in a ratio of 0.2−0.5 gave $\delta^{98/95}$Mo = 0.00 ± 0.07‰ (2SD, n = 16) relative to NIST SRM 3134 (Zhang et al., 2018). $\delta^{98/95}$Mo values of -0.61 ± 0.02‰ (2 SE, n = 4) and -0.25 ± 0.02‰ (2 SE, n = 4) were obtained for BGW 07-316 and COQ-1, respectively. These results are consistent with previously reported values (Li et al., 2014; Zhao et al., 2016). The procedural blank was 0.60 ± 0.76 ng Mo (2 SD, n = 4), far less than the total Mo content of samples. Values of $\delta^{98/95}$Mo for our samples relative to NIST SRM 3134 (0.25‰; Nägler et al., 2014) were calculated as follows:

$$\delta^{98/95}\text{Mo (‰)} = \left(\frac{(^{98/95}\text{Mo})_{\text{sample}}}{(^{98/95}\text{Mo})_{\text{NIST3134}} * 0.99975} - 1\right) * 1000$$

5. Carbon isotopes

The fifty sample powders chosen for Mo isotopic analysis were also analysed for carbonate carbon ($\delta^{13}C_{carb}$) and oxygen ($\delta^{18}O$) isotopes by Iso-Analytical Limited. Samples were reacted with phosphoric acid in Exetainer™ tubes and heated at 90°C for 3 h, then left to react at room temperature for 24 h for complete conversion of carbonate to CO_2. Carbon and oxygen isotopic compositions of the liberated CO_2 were then measured by Continuous Flow-Isotope Ratio Mass Spectrometry (CF-IRMS) on a Europa Scientific 20-20 IRMS. Isotopic compositions are reported relative to the Vienna Pee Dee Belemnite (VPDB) standard. Reference materials used during the analyses included NBS-18 (carbonatite; $\delta^{13}C_{VPDB}$ = -5.01‰ and $\delta^{18}O_{VPDB}$ = -23.2‰), which is an inter-laboratory standard material distributed by the International Atomic Energy Agency (IAEA), as well as laboratory standards IA-R022 (calcium carbonate; $\delta^{13}C_{VPDB}$ = -28.63‰ and $\delta^{18}O_{VPDB}$ = -22.69‰), IA-R066 (chalk; $\delta^{13}C_{VPDB}$ = +2.33‰ and $\delta^{18}O^{VPDB}$ = -1.52‰), IA-R040 (dolomite; $\delta^{13}C_{VPDB}$ = -0.72‰ and $\delta^{18}O_{VPDB}$ = -17.07‰) and ILC1 (limestone; $\delta^{13}C_{VPDB}$ = +2.17‰ and $\delta^{18}O_{VPDB}$ = -3.99‰). Acid preparations of samples and controls were measured directly against acid preparations of the working calcium carbonate standard (IA-R022), which removes the need to apply separate corrections for temperature dependent isotope fractionation. For C isotope measurements, accuracy was determined as >97% with a precision of <3%, while for O isotope measurements, accuracy was determined as >99% with a precision of <3%.

Model Assumptions

The modelling approach involves a number of assumptions, including:

1) **The ocean is well-mixed with respect to Mo and the analysed δ^{98}Mo reflects a homogeneous seawater composition**. We use an updated database of Mo concentrations from shale samples that have been independently constrained (using Fe-speciation and Fe/Al, degree of pyritization and redox sensitive trace metal enrichments) as having been deposited under euxinic bottom water conditions to estimate Mesoproterozoic seawater [Mo]. This database builds on the shale database of Scott et al. (2008) and Reinhard et al. (2013) through addition of more recent Mesoproterozoic geochemical data (Gilleaudeau and Kah, 2013; Yang et al., 2017; Zhang et al., 2019; Diamond et al., 2018). Under ideal conditions, where aqueous H_2S is sufficiently elevated (>11 μM) to result in near-quantitative Mo drawdown, shale Mo concentrations may approach the homogeneous seawater [Mo]. This is best exemplified in the modern ocean by sediments deposited under euxinic conditions in the Cariaco basin, which is openly connected to the global ocean. Here, sediments record Mo concentrations of up to 80% of the homogeneous seawater concentration (Scott et al., 2008). It is likely that euxinic intervals in the Mesoproterozoic ocean were characterised by relatively low H_2S_{aq}, and in this case the Mo concentrations of euxinic shales represent a minimum estimate of seawater [Mo]. Scott et al. (2008) investigated bulk shale and dissolved Mo concentrations, in addition to Mo/TOC, to estimate the Mo burial efficiency in modern openly-connected euxinic basins. Scaling the mean Mo concentration from the Mesoproterozoic euxinic shale database to the modern estimate of Mo burial efficiency yields a Mesoproterozoic [Mo] of ~21 nM (Scott et al., 2008). This is consistent with the ~2 – 0.6 Ga estimate of Scott et al. (2008), who extrapolated a Mo residence time for the Proterozoic ocean of <150 kyrs. Uncertainties in this calculation are associated with potential catagenic loss of organic matter (affecting Mo/TOC), the aforementioned non-quantitative Mo drawdown expected under lower Mesoproterozoic H_2S_{aq}, in

addition to the possibility for a smaller riverine Mo flux and/or larger hydrothermal Mo flux at 1.56 Ga (Kendall et al., 2009, 2011). However, despite this large uncertainty, the estimate of 150 kyrs is far greater than the modern ocean mixing time of ~1500 years.

2) **The local depositional environment is well connected to the global ocean.** In a semi-restricted environment with deep water anoxia, the average δ^{98}Mo composition of local seawater would approach the composition of the riverine source (Dahl et al., 2010). In the absence of a robust global chemostratigraphic framework tied to reliable radiometric age constraints, the degree of connection between the Yanliao basin and the global ocean is difficult to assess. However, inter-section carbon isotope chemostratigraphy alongside sequence stratigraphy is well constrained and consistent across distances of up to 200 km in the Yanliao Basin, and previously published rare earth element data for upper Gaoyuzhuang Member III and Member IV show typical oxic marine profiles (Zhang et al., 2018). The sedimentary architecture, including observed facies variability in addition to changes in interpreted depositional depth throughout the timescale of deposition are most parsimoniously interpreted as reflecting open marine carbonate deposition with accommodation space changes under partial eustatic control (Chen et al., 1981; Chu et al., 2007).

3) **Rivers are the dominant source of Mo to the oceans, and the δ^{98}Mo composition of riverine material is comparable to upper continental crust.** This assumes that, on timescales shorter than the oceanic residence time, most/all soil-bound Mo is released. It also assumes that the Mo contribution from low-temperature hydrothermal input is negligible. The importance of changes in the fractional contribution and isotopic composition of low-temperature hydrothermal fluids throughout deep time, and the removal of this component, remains one of the largest uncertainties in the model. Here, we use a conservative range of δ_{INPUT} between 0.4 and 0.7‰, which falls well

within the compositional range of δ^{98}Mo from riverine input and analyses of upper continental crust and molybdenite (Siebert et al., 2003; Archer and Vance, 2008; Dahl et al., 2010; Kendall et al., 2011).

4) **The isotopic fractionation associated with Mo removal under anoxic non-euxinic conditions in the Mesoproterozoic ocean was dominated by the fractionation factor associated with adsorption onto ferrihydrite.** This assumption leads to estimations of the isotopic fractionation of reducing non-euxinic environments in the range 0.9 – 1.1‰ based on experimental laboratory studies (Goldberg et al., 2009).

5) **Incorporation of molybdate into the carbonate lattice is thought to be accompanied by negligible isotopic fractionation.** Some studies report that maximum δ^{98}Mo values in non-biogenic carbonates and stromatolites approximate seawater δ^{98}Mo (Voegelin et al., 2009; Thoby et al., 2019). One complication involves Mo fractionation associated with incorporation of Mn during penecontemporaneous carbonate crystal growth or during later diagenetic incorporation at any point prior to full pore occlusion. The leaching protocol used herein (6 M HCl) may also non-quantitatively leach some detrital minerals and organics (Clarkson et al., 2020). Whilst these samples have undergone chromatographic purification for Mo, the presence of Fe and Mn oxides may have led to δ^{98}Mo fractionation during early diagenesis, as discussed in detail in the main text. For this reason, we have screened samples prior to δ^{98}Mo assessment, and only consider samples from Gaoyuzhuang Member IV. We note that many, if not all, of the remaining samples show strong evidence for Mo isotopic fractionation during diagenesis. Figure 4 shows the samples that we consider to best preserve seawater δ^{98}Mo.

References

Alcott, L. J., Krause, A. J., Hammarlund, E. U., Bjerrum, C. J., Scholz, F., Xiong, Y.J, Hobson, A.J., Neve, L., Mills, B.J.W., März, C., Schnetger, B., Bekker, A., Poulton, S. W., 2020. Development of iron speciation reference materials for palaeoredox analysis. Geostandards and Geoanalytical Research, 44, 581-591.

Archer, C., Vance, D. 2008. The isotopic signature of the global riverine molybdenum flux and anoxia in the ancient oceans. Nature Geoscience 1(9), 597-600.

Benkovitz, A., Matthews, A,, Teutsch, N., Poulton, S.W., Bar-Matthews. M., Almogi-Labin, A. 2020. Tracing water column euxinia in Eastern Mediterranean Sapropels S5 and S7. Chemical Geology 545, 119627.

Canfield, D.E., Raiswell, R., Westerich, J.T., Reaves, C.M., Berner, R., A., 1986. The use of chromium reduction in the analysis of reduced inorganic sulfur in sediments and shales. Chemical Geology 54, 149-155.

Clarkson, M.O., Poulton, S.W., Guilbaud, R., Wood, R.A., 2014. Assessing the utility of Fe/Al and Fe-speciation to record water column redox conditions in carbonate-rich sediments. Chemical Geology 382, 111-122.

Clarkson, M.O., Musing, K., Andersen, M.B., Vance, D., 2020. Examining pelagic carbonate-rich sediments as an archive for authigenic uranium and molybdenum isotopes using reductive cleaning and leaching experiments. Chemical Geology 539, 199412.

Dahl, T.W., Hammarlund, E.U., Anbar, A.D., Bond, D.P.G., Gill, B.C., Gordon, G.W., Knoll, A.H., Nielsen, A.T., Schovsbo, N.H., Canfield, D.E., 2010. Devonian rise in atmospheric oxygen correlated to the radiations of terrestrial lants and large predatory fish. National Academy of Sciences Proceedings 107, 17911-17915.

Goldberg, T., Archer, C., Vance, D., Poulton, S.W., 2009. Mo isotope fractionation during adsorption to Fe (oxyhydr) oxides. Geochimica et Cosmochimica Acta 73, 6502-6516.

Kendall, B., Creaser, R.A., Gordon, G.W., Anbar, A.D., 2009. Re–Os and Mo isotope systematics of black shales from the Middle Proterozoic Velkerri and Wollogorang Formations, McArthur Basin, northern Australia. Geochimica et Cosmochimica Acta 73, 2534-2558.

Kendall, B., Gordon, G.W., Poulton, S.W., Anbar, A.D., 2011. Molybdenum isotope constraints on the extent of late Paleoproterozoic ocean euxinia. Earth and Planetary Science Letters 307, 450-460.

Li, J., Liang, X.R., Zhong, L.F., Wang, X.C., Ren, Z.Y., Sun, S.L., Zhang, Z.F., Xu, J.F., 2014. Measurement of the isotopic composition of molybdenum in geological samples by MC-ICP-MS using a novel chromatographic extraction technique. Geostandards and Geoanalytical Research 38, 345-354.

Nägler, T.F., Anbar, A.D., Archer, C., Goldberg, T., Gordon, G.W., Greber, N.D., Siebert, C., Sohrin, Y., Vance, D., 2014. Proposal for an international molybdenum isotope measurement standard and data representation. Geostandards and Geoanalytical Research 34, 149-151.

Poulton, S.W., Canfield, D.E., 2011. Ferruginous conditions: a dominant feature of the ocean through Earth's history. Elements 7, 107-112.

Poulton, S. W., 2020. The iron speciation paleoredox proxy. In Geochemical Tracers in Earth System Science (eds. T. Lyons, A. Turchyn, C. Reinhard), Cambridge University Press, in press.

Raiswell, R., Canfield, D.E., 1998. Sources of Iron for Pyrite. American Journal of Science 298, 219–245.

Scott, C., Lyons, T.W., Bekker, A., Shen, Y., Poulton, S.W., Chu, X.L., Anbar, A.D., 2008. Tracing the stepwise oxygenation of the Proterozoic ocean. Nature 452, 456-459.

Shang, M.H., Tang, D.J., Shi, X.Y., Zhou, L.M., Zhou, X.Q., Song, H.Y., Jiang, G.Q., 2019. A pulse of oxygen increase in the early Mesoproterozoic ocean at ca. 1.57–1.56 Ga. Earth and Planetary

Science Letters 527, 115797.

Siebert, C., Nagler, T.F., Blanckenburg, F.v., Kramers, J.D., 2003. Molybdenum isotope records as a potential new proxy for paleoceanography. Earth and Planetary Science Letters 211, 159-171.

Thoby, M., Konhauser, K.O., Fralick, P.W., Altermann, W., Visscher, P.T., Lalonde, S.V., 2019. Global importance of oxic molybdenum sinks prior to 2.6 Ga revealed by the Mo isotope composition of Precambrian carbonates. Geology 47, 559-562.

Voegelin, A.R., Nagler, T.F., Samankassou, E., Villa, I.M., 2009. Molybdenum isotopic composition of modern and carboniferous carbonates. Chemical Geology 265, 488-498.

Zhang, K., Zhu, X.K., Wood, R.A., Shi, Y., Gao, Z.F., Poulton, S.W., 2018. Oxygenation of the Mesoproterozoic ocean and the evolution of complex eukaryotes. Nature Geocisence 11, 1110-1120.

Zhang, L., Ren, Z.Y., Xia, X.P., Li, J., Zhang, Z.F., 2015. IsotopeMaker: A Matlab program for isotopic data reduction. International Journal of Mass Spectrometry 392, 118-124.

Zhao, P.P., Li, J., Zhang, L., Wang, Z.B., Kong, D.X., Ma, J.L., Wei, G.J., Xu, J.F., 2015. Molybdenum mass fractions and isotopic compositions of international geological reference materials. Geostandards and Geoanalytical Research 40, 217-226.